

Open bottom states and the \bar{B} -meson propagation in hadronic matter

Juan M. Torres-Rincon

*Institut de Ciències de l'Espai (IEEC/CSIC), Campus Universitat Autònoma de Barcelona,
Facultat de Ciències, Torre C5, E-08193 Bellaterra, Spain and
Subatech, UMR 6457, IN2P3/CNRS, Université de Nantes,
École de Mines de Nantes, 4 rue Alfred Kastler 44307, Nantes, France*

Laura Tolos

*Institut de Ciències de l'Espai (IEEC/CSIC), Campus Universitat Autònoma de Barcelona,
Facultat de Ciències, Torre C5, E-08193 Bellaterra, Spain and
Frankfurt Institute for Advanced Studies. Johann Wolfgang Goethe University,
Ruth-Moufang-Str. 1, 60438 Frankfurt am Main, Germany*

Olena Romanets

KVI, University of Groningen, Zernikelaan 25, 9747AA Groningen, The Netherlands

(Dated: September 27, 2018)

The interaction and propagation of \bar{B} mesons with light mesons, N and Δ is studied within a unitarized approach based on effective models that are compatible with chiral and heavy-quark symmetries. We find several heavy-quark spin doublets in the open-bottom sectors, where \bar{B} and \bar{B}^* mesons are present. In the meson sector we find several resonant states, among them, a B_0 and a B_1 with masses 5530 MeV and 5579 MeV as well as B_{s0}^* and B_{s1}^* narrow states at 5748 MeV and 5799 MeV, respectively. They form two doublets with no experimental identification yet, the first one being the bottom counterpart of the $D_0(2400)$ and $D_1(2430)$ states, and the second bottom doublet associated to the ubiquitous $D_{s0}^*(2317)$ and the $D_{s1}(2460)$. In the baryon sector, several Λ_b and Σ_b doublets are identified, among them the one given by the experimental $\Lambda_b(5910)$ and $\Lambda_b^*(5921)$. Moreover, one of our states, the $\Sigma_b^*(5904)$, turns out to be the bottom counterpart of the $\Sigma^*(1670)$ and $\Sigma_c^*(2549)$, which is a case for discovery. We finally analyze different transport coefficients for the \bar{B} meson in hot matter, such as formed in heavy-ion collisions at RHIC and LHC. For RHIC/LHC energies, the main contribution to the coefficients comes from the interaction of \bar{B} mesons with pions. However, we also include the effects of baryonic density which might be sizable at temperatures $T \lesssim 100$ MeV, as the chemical potential is expected to increase in the last stages of the expansion. We conclude that although the relaxation time decreases with larger baryonic densities, the \bar{B} meson does not thermalize at RHIC/LHC energies, representing an ideal probe for the initial bottom distribution.

PACS numbers: 14.40.Nd,12.39.Fe,12.39.Hg,11.10.St,51.20.+d

I. INTRODUCTION

The properties of matter created in heavy-ion collisions (HICs) have been a subject of interest over the past decades. Most of the studies have been focused in the potential signatures and features of the deconfined phase, the quark-gluon plasma (QGP). For the characterization of this phase, hadrons with heavy flavor (charm or bottom) play a fundamental role as heavy quarks, produced in the early stage of the collision, can probe the formed medium during its entire evolution. When the medium cools down, the hadronization takes place and, after freeze-out, heavy-flavored hadrons are finally detected [1]. Therefore, heavy hadrons –such as D and B mesons– are considered to be an efficient and unique probe for testing the hot and dense medium created in HICs, in both QGP and hadronic phases.

Focusing on the latter, the diffusion of D mesons in hadronic matter was initially obtained within an effective theory that incorporates both chiral and heavy-quark symmetries [2] and also using parametrized interactions

with light mesons and baryons [3]. Moreover, effective Lagrangians at leading order were used to obtain the scattering amplitudes of D mesons with light mesons and baryons [4]. However, the need of unitarization was later pointed out in order to avoid unphysical large transport coefficients [5] and also next-to-leading order contributions were considered [5–7].

More recently, the propagation of bottom mesons in matter, such as B mesons has been analyzed. The drag and diffusion coefficients of open bottom mesons in a hadronic medium of pions, kaons and etas was evaluated with the use of scattering lengths as dynamical input [8]. In that work, inelastic channels and non-perturbative processes were not taken into account. The non-perturbative character of the B meson interaction in a mesonic environment was addressed in Ref. [9], and it was found to be relevant for the determination of the transport coefficients, as in the case of D mesons.

In this paper we aim at, first, analyzing the scattering of \bar{B} mesons with light mesons and baryons, such as N and Δ , within a unitarized approach in coupled

channels taking, as bare interaction, effective models that are compatible with chiral and heavy-quark symmetries. Note that in this paper we study the \bar{B} meson, the counterpart of the D meson in the bottom sector. In the meson sector, we extend the results of Ref. [9] including the coupled-channel structure of the interaction of \bar{B} with pions, kaons, anti-kaons and etas (by also incorporating the interaction of B_s with light mesons in the coupled channel structure). In the baryonic sector, we continue the study initiated in Ref. [10] with regard to the open-bottom baryon states in order to determine the scattering of \bar{B} mesons with N and Δ . We then obtain the transport coefficients for a \bar{B} meson in this hadronic environment by making use of our previous knowledge of the scattering of \bar{B} mesons in matter. We present results for the diffusion and drag coefficients at zero baryochemical potential which can be used in transport calculations for high-energy collisions, such as those at the Relativistic Heavy Ion Collider (RHIC) [11] or the Large Hadron Collider (LHC) [12]. Afterwards, we discuss the behavior of the relaxation time and the spatial diffusion coefficient for isentropic trajectories ranging from RHIC/LHC conditions to FAIR [13] at its top energy.

The paper is organized as follows. In Sec. II we study the interaction of \bar{B} mesons with light mesons, nucleons and Δ within unitarized effective theories and present the dynamically-generated open bottom states. In Sec. III we introduce the relevant transport coefficients for heavy mesons and present our results as a function of temperature, baryochemical potential (or entropy per baryon) and the momentum of the heavy meson. Our conclusions are given in Sec. IV.

II. OPEN BOTTOM STATES

In this section we study the interaction of \bar{B} mesons with hadrons within a unitarized approach in coupled-channels based on effective models that are compatible with chiral and heavy quark symmetries, in particular heavy-quark spin symmetry (HQSS). The unitarization in coupled channels has proven to be very successful in describing some of the existing experimental data on baryon and meson states as dynamically generated states. These are obtained as poles of the scattering amplitudes in coupled-channel basis, that is usually characterized by different quantum numbers, such as bottom (B), charm (C), strange (S), isospin (I) and spin (J). We concentrate on the sectors with $B = -1$ and $C = 0$, where \bar{B} (and also \bar{B}^*) mesons interact with light mesons as well as N and Δ baryons.

The scattering amplitudes T for the interaction of \bar{B} mesons with light mesons and baryons follows the standard multichannel scattering (integral) Bethe-Salpeter (BS) equation,

$$T = V + VGT, \quad (1)$$

where V is the potential resulting from the meson-meson

(baryon-meson) effective Lagrangian and G is the two-particle meson-meson (baryon-meson) propagator.

The kernel V is a matrix that consists of all possible meson-meson (baryon-meson) transitions. We focus on the interaction of \bar{B} mesons with the pseudo-Goldstone bosons (π , K , \bar{K} and η) as well as with the lightest baryons (N and Δ). We make use of the effective model of Ref. [5, 9] for the interaction of \bar{B} mesons with light mesons, which is consistent with chiral and heavy-quark symmetries. For the scattering of \bar{B} mesons with baryons, we take into account the $SU(6) \times HQSS$ WT scheme of Refs. [10, 14–17]. Similarly to the meson-meson sector, the baryon-meson model fulfills chiral symmetry in the light-quark sector while heavy-quark symmetry constraints are respected in the heavy-quark sector. The details of these effective models will be given in the Secs. II A and II B.

The V kernel can be factorized in the on-mass shell [18], so the scattering amplitudes T of Eq. (1) are the solutions of a set of linear algebraic coupled equations

$$T_{ij} = [1 - VG]_{ik}^{-1} V_{kj}, \quad (2)$$

where i and j indicate the initial meson-meson (baryon-meson) and final meson-meson (baryon-meson) systems, respectively. This approach is practically equivalent to the so-called N/D method [19]. In the on-shell *ansatz*, the two-particle propagators—often called loop functions—form a diagonal matrix G . The loop function reads

$$G_r(\sqrt{s}) = i\gamma_r \int \frac{d^4q}{(2\pi)^4} \frac{1}{(P-q)^2 - M_r^2 + i\epsilon} \frac{1}{q^2 - m_r^2 + i\epsilon}, \quad (3)$$

with the total four-momentum P related to the center-of-mass (C.M.) squared energy s by $s = P^2$, and q being the relative four-momentum in the center-of-mass frame. The quantities m_r and M_r stand for the masses of the two particles propagating in the intermediate channel r , i.e., two mesons, or a meson and a baryon. The factor γ_r has been introduced to account for the different normalization of the meson-meson and baryon-meson interactions. In fact, as we will see in the following subsections, $\gamma_r = 1$ for the adimensional meson-meson V kernel while for the baryon-meson sector $\gamma_r = 2M_r$, with M_r being the mass of the baryon. The meson-meson (baryon-meson) loop functions are divergent and are regularized by means of dimensional regularization.

In order to study the dynamically-generated resonances, we study both the first and second Riemann sheets of the C.M. energy \sqrt{s} . The poles of the scattering amplitude on the first Riemann sheet that appear on the real axis below threshold are interpreted as bound states. The poles that are found on the second Riemann sheet below the real axis and above threshold are identified with resonances. Note that we often refer to all poles generically as resonances, regardless of their concrete nature, since usually they can decay through other channels not included in the model space. The mass and the width

of the bound state/resonance can be found from the position of the pole on the complex energy plane. Close to the pole, the T -matrix behaves as

$$T_{ij}(s) \approx \frac{g_i e^{i\phi_i} g_j e^{i\phi_j}}{z(s) - z_R}. \quad (4)$$

where, in the baryon-meson sector, $z(s) = \sqrt{s}$ and $z_R = M_R - i\Gamma_R/2$ provides the mass (M_R) and the width (Γ_R) of the resonance, while $g_j e^{i\phi_j}$ (modulus and phase) is the (adimensional) coupling of the resonance to the channel j . In the usual parametrization for the meson-meson scattering, $z(s) = s$ and z_R is the pole position in the s plane with a coupling with dimensions of energy.

A. Bottom meson resonances

The interaction between the \bar{B} mesons and the pseudoscalar Goldstone bosons is given by the effective Lagrangian in Refs [5, 20–23]. In particular we adapt the B -meson interaction from our past work [9] to the present case, where the \bar{B} field is given by $\bar{B} = (B^-, \bar{B}^0, \bar{B}_s^0)$.

At leading-order (LO) in heavy-quark mass expansion and next-to-leading order (NLO) in the chiral expansion the tree-level scattering amplitude of a \bar{B} meson interacting with light mesons reads

$$V^{IJSB} = \frac{C_0}{4f_\pi^2}(s - u) + \frac{2C_1 h_1}{3f_\pi^2} + \frac{2C_2}{f_\pi^2} h_3(p_2 \cdot p_4) \quad (5)$$

$$+ \frac{2C_3}{f_\pi^2} h_5[(p_1 \cdot p_2)(p_3 \cdot p_4) + (p_1 \cdot p_4)(p_2 \cdot p_3)],$$

where p_1 and p_2 are the four-momenta of the incoming hadrons, p_3 and p_4 the outgoing momenta, and $s = (p_1 + p_2)^2$ and $u = (p_1 - p_4)^2$. At LO in the heavy-quark expansion, the scattering amplitude for \bar{B}^* meson with light mesons coincides (modulus the polarization vectors) with the amplitude of Eq. (5). For completeness, we will thus also show the results in the $J = 1$ channel, with the only heavy-quark breaking effect being the physical masses of the bottom mesons.

The quantities C_i are the isospin coefficients of the different scattering amplitudes of \bar{B} mesons with π , K , \bar{K} and η mesons, which are shown in Table I. The h_i coefficients are the low-energy constants (LECs). We fix $h_1 = -1.042$ using the mass difference between the B and B_s mesons [23], whereas h_3 and h_5 are free. With the inclusion of all coupled channels and the analysis of the scattering amplitudes in the whole complex plane we have found that the previously used values of h_3 and h_5 provided a too large NLO contribution with respect to LO. We recalibrate h_3 and h_5 keeping a more conservative (smaller) values. The numbers we use are $h_3 = 0.25$ and $h_5 = -0.015 \text{ GeV}^{-2}$. In order to solve the BS equation of Eq. (1), the loop function needs to be renormalized. We keep the prescription of Ref. [9], which consists on fixing the value of the loop function in dimensional regularization at $\mu = 1 \text{ GeV}$ to the one coming from cutoff

regularization for $\Lambda = 770 \text{ MeV}$ at the energy threshold of the lightest channel, $m_B + m_\pi$. In this case, the subtraction constant is set to $a(\mu) = -3.38$. In fact, as we shall see, the combination of the free LECs and the subtraction constant are determined to reproduce a state, B_0 , with a similar mass of that found in Ref. [9].

1. B states ($J = 0$)

In Table II we show the mass and width of the different $J = 0$ states in the $B = -1$ sector together with their couplings to the different meson-meson channels and the meson-meson channels that are allowed for decay. The resonance in the $(S, I) = (0, 1/2)$ sector at 5530 MeV is assigned to a wide B_0 resonance (not yet experimentally seen) in analogy to the experimental $D_0(2400)$ in the charm sector [24].¹

In Ref. [25] this resonant state is seen at 5536 MeV with a width of 234 MeV using a similar method at LO in the chiral expansion. Within the non-linear chiral SU(3) model of [26], this state is located at 5526 MeV but no width is provided. We also observe a second narrower resonance in $(S, I) = (0, 1/2)$ at 5827 MeV, which was overlooked in [9]. This state is identified in [25] with $M_R = 5842 \text{ MeV}$ and $\Gamma = 35 \text{ MeV}$, and with $M_R = 5760 \text{ MeV}$ and a width of approximately 30 MeV in [26]. Moreover, we find two narrow states. The first one at 5748 MeV is seen in the $(1, 0)$ channel, that mainly couples to $\bar{B}K$ channel. In Ref. [25] it is located at 5729 MeV while in Ref. [26] it is found at 5643 MeV. The state in the $(S, I) = (-1, 0)$ channel lies at 5774 MeV, close to the bound state found in [26]. No state is seen in the $(S, I) = (1, 1)$ channel, in contrast to the findings of [26].

2. B^* states ($J = 1$)

We show in Table III the $J = 1$ states. Two wide resonances are found with masses 5579 MeV and 5880 MeV that couple strongly to $\bar{B}^*\pi$ and $\bar{B}_s^*\bar{K}$, respectively. The first one is the charm counterpart of the $D_1(2430)$ state. Furthermore, two narrow states at 5799 MeV and 5820 MeV are seen, with a strong coupling to $\bar{B}^*\bar{K}$.

In Ref. [26] is also found that the 1^+ spectrum resembles the 0^+ sector, predicting states at 5590 MeV and 5810 MeV $(S, I) = (0, 1/2)$, 5690 MeV for $(S, I) = (1, 0)$, 5807 MeV in $(S, I) = (-1, 0)$, and 5790 MeV in $(S, I) = (1, 1)$. We generate similar states to those reported in Ref. [26], with the exception of the resonance in the $(S, I) = (1, 1)$ sector. In Ref. [27], a bound state with mass of 5778 MeV was obtained in the $(S, I) = (1, 0)$

¹ The amplitudes of B and \bar{B} mesons interacting with light mesons at LO in the heavy-quark mass expansion and NLO in the chiral expansion are related by charge conjugation.

(S, I)	Channel	C_0	C_1	C_2	C_3
$(0, \frac{1}{2})$	$\bar{B}\pi \rightarrow \bar{B}\pi$	-2	$-3m_\pi^2$	1	1
	$\bar{B}\pi \rightarrow \bar{B}\eta$	0	$-3m_\pi^2$	1	1
	$\bar{B}\eta \rightarrow \bar{B}\eta$	0	$-m_\pi^2$	1/3	1/3
	$\bar{B}_s\bar{K} \rightarrow \bar{B}_s\bar{K}$	-1	$-3m_K^2$	1	1
	$\bar{B}\pi \rightarrow \bar{B}_s\bar{K}$	$-\sqrt{6}/2$	$-3\sqrt{6}(m_K^2 + m_\pi^2)/4$	$\sqrt{6}/2$	$\sqrt{6}/2$
$(0, \frac{3}{2})$	$\bar{B}\eta \rightarrow \bar{B}_s\bar{K}$	$-\sqrt{6}/2$	$\sqrt{6}(5m_K^2 - 3m_\pi^2)/4$	$-\sqrt{6}/6$	$-\sqrt{6}/6$
	$\bar{B}\pi \rightarrow \bar{B}\pi$	1	$-3m_\pi^2$	1	1
$(1, 0)$	$\bar{B}K \rightarrow \bar{B}K$	-2	$-6m_K^2$	2	2
	$\bar{B}_s\eta \rightarrow \bar{B}_s\eta$	0	$-2(3m_\eta^2 - m_\pi^2)$	4/3	4/3
$(1, 1)$	$\bar{B}K \rightarrow \bar{B}_s\eta$	$-\sqrt{3}$	$-\sqrt{3}(5m_K^2 - 3m_\pi^2)/2$	$\sqrt{3}/3$	$\sqrt{3}/3$
	$\bar{B}K \rightarrow \bar{B}K$	0	0	0	0
	$\bar{B}_s\pi \rightarrow \bar{B}_s\pi$	0	0	0	0
$(-1, 0)$	$\bar{B}K \rightarrow \bar{B}_s\pi$	1	$-3(m_K^2 + m_\pi^2)/2$	1	1
	$\bar{B}\bar{K} \rightarrow \bar{B}\bar{K}$	-1	$3m_K^2$	-1	-1
$(-1, 1)$	$\bar{B}\bar{K} \rightarrow \bar{B}\bar{K}$	1	$3m_K^2$	1	1
$(2, \frac{1}{2})$	$\bar{B}_sK \rightarrow \bar{B}_sK$	1	$-3m_K^2$	1	1

TABLE I: Isospin coefficients of the scattering amplitudes for the \bar{B} meson-light meson channels with total strangeness S and isospin I .

M_R (MeV)	Γ_R (MeV)	Couplings to main channels (MeV ^{1/2})	(S, I)	Open channels
5530.3	238.5	$g_{\bar{B}\pi} = 25.3, g_{\bar{B}\eta} = 2.5, g_{\bar{B}_s\bar{K}} = 11.5$	(0,1/2)	$\bar{B}\pi$
5827.0	48.1	$g_{\bar{B}\pi} = 6.7, g_{\bar{B}\eta} = 16.1, g_{\bar{B}_s\bar{K}} = 26.2$	(0,1/2)	$\bar{B}\pi, \bar{B}\eta$
5747.6	0.0	$g_{\bar{B}K} = 19.9, g_{\bar{B}_s\eta} = 13.9$	(1,0)	
5774.0	0.2	$g_{\bar{B}\bar{K}} = 7.1$	(-1,0)	$\bar{B}\bar{K}$

TABLE II: Masses, widths and couplings to meson-meson channels of the \bar{B} resonances ($J = 0$). In the first and second column we present the mass and width of these states, respectively. The next column displays the (modulus of the) couplings to the different meson-meson channels, ordered by threshold energies. The fourth column indicates the strangeness (S) and isospin (I) of the resonance while in the last column we show the meson-meson channels that are allowed for decay.

sector, similar to our bound state at 5799 MeV. In the $(S, I) = (1/2, 0)$ channel, two states were found in [27] with masses similar to ours. The $(S, I) = (-1, 0)$ sector was not explored in Ref. [27].

Note that at LO in heavy-quark expansion, the $J = 0$ and $J = 1$ sectors are decoupled [9] and that an analogous set of states to the $J = 0$ sector is obtained due to HQSS. In fact, the $J = 0$ and $J = 1$ states form HQSS doublets. We define a HQSS doublet as a pair of $J = 0$ and $J = 1$ states that are degenerate when HQSS is restored. Such states have similar masses, with the $J = 0$ state coupling strongly to a two-particle channel with one of the intervening particles being the HQSS partner of one of the particles in the dominant two-particle channel for the generation of the $J = 1$ state. This is the case, for example, of the $B_0(5530)$ and $B_1(5579)$, which turn out to be the bottom counterparts of the experimental $D_0(2400)$ and $D_1(2430)$, as well as the $B_{s0}^*(5748)$ and $B_{s1}^*(5799)$, these last two possibly being the bottom homologues of the $D_{s0}^*(2317)$ and the $D_{s1}(2460)$ states, respectively.

B. Bottom baryon resonances

We follow here the approach applied in Refs. [14–17] for charm quarks and recently used in the bottom sector [10]. The model obeys SU(6) spin-flavor symmetry and also HQSS [17]. This is a model extension of the WT SU(3) chiral Lagrangian [14, 16]. The extended SU(6)×HQSS WT baryon-meson interaction is given by

$$V_{ij}^{IJSB}(s) = \frac{D_{ij}^{IJSB}}{4 f_i f_j} (2\sqrt{s} - M_i - M_j) \times \sqrt{\frac{M_i + E_i}{2M_i}} \sqrt{\frac{M_j + E_j}{2M_j}}. \quad (6)$$

The i (j) are the outgoing (incoming) baryon-meson channels while M_i , E_i and f_i stand for the baryon mass and energy, in the C.M. frame, and the meson decay constant in the i channel, respectively. The masses of baryons with bottom content used in this work are compiled in Tables I of Ref. [10], while those of the bottom mesons and their decay constants are given in Table II of Ref. [10]. The rest of hadron masses and meson decay

M_R (MeV)	Γ_R (MeV)	Couplings to main channels (MeV ^{1/2})	(S, I)	Open channels
5579.2	251.9	$g_{\bar{B}^*\pi} = 25.9, g_{\bar{B}^*\eta} = 2.9, g_{\bar{B}^*_s\bar{K}} = 12.0$	(0,1/2)	$\bar{B}^*\pi$
5880.4	53.0	$g_{\bar{B}^*\pi} = 6.5, g_{\bar{B}^*\eta} = 15.3, g_{\bar{B}^*_s\bar{K}} = 25.1$	(0,1/2)	$\bar{B}^*\pi, \bar{B}^*\eta$
5798.7	0.0	$g_{\bar{B}^*K} = 19.3, g_{\bar{B}^*_s\eta} = 13.9$	(1,0)	
5820.0	0.7	$g_{\bar{B}^*\bar{K}} = 9.8$	(-1,0)	$\bar{B}^*\bar{K}$

TABLE III: As in Table II, but for B^* meson resonances ($J = 1$).

constants have been taken from Ref. [16]. The D_{ij}^{IJSB} elements are the coefficients coming from the underlying SU(8) group structure in the Appendix B of Ref. [16], where one can identify the charm $C = 1$ sector couplings given there with those needed here that correspond to the $B = -1$ sector.

In order to solve the BS equation of Eq. (1), the loop function is renormalized by a subtraction constant such that

$$G_r^{IJS} = 0 \quad \text{at} \quad \sqrt{s} = \mu^{IS}. \quad (7)$$

To fix the subtraction point μ^{IS} we apply the following prescription: μ^{IS} is independent of J and is taken as $\sqrt{m_{\text{th}}^2 + M_{\text{th}}^2}$, where m_{th} and M_{th} , are respectively, the masses of the meson and baryon producing the lowest threshold (minimal value of $m_{\text{th}} + M_{\text{th}}$).

We concentrate on all $B = -1$ sectors where \bar{B} mesons interact with N and Δ since we are interested in studying the propagation of \bar{B} in a hadronic environment. These are the Λ_b and Λ_b^* ($I = 0; J = 1/2, 3/2$), the Σ_b and Σ_b^* ($I = 1; J = 1/2, 3/2$) and the ($I = 2; J = 3/2$) sectors. Note that the vacuum Δ -decay width has to be considered for the determination of the dynamically-generated resonances. This effect is introduced in the unitarization procedure through a convolution of the \bar{B} Δ propagator with the corresponding spectral function of the Δ baryon, as done in Ref. [15]. Only the resonances that lie close to the \bar{B} Δ channel, as compared to the Δ width, and that couple strongly to this system will be affected.

1. Λ_b and Λ_b^* states ($I = 0; J = 1/2, 3/2$)

In the Λ_b sector, the following sixteen channels are involved:

$$\begin{array}{cccccccc} \Sigma_b\pi & \Lambda_b\eta & N\bar{B} & N\bar{B}^* & \Xi_b K & \Lambda_b\omega & \Xi'_b K & \Lambda\bar{B}_s^0 \\ \Lambda\bar{B}_s^* & \Lambda_b\eta' & \Sigma_b\rho & \Sigma_b^*\rho & \Lambda_b\phi & \Xi_b K^* & \Xi'_b K^* & \Xi_b^* K^* \end{array}$$

Likewise for the Λ_b^* sector, there are eleven channels:

$$\begin{array}{ccccccc} \Sigma_b^*\pi & N\bar{B}^* & \Lambda_b\omega & \Xi_b^* K & \Lambda\bar{B}_s^* & \Sigma_b\rho & \\ \Sigma_b^*\rho & \Lambda_b\phi & \Xi_b K^* & \Xi'_b K^* & \Xi_b^* K^* & & \end{array}$$

In both cases the channels are ordered by increasing mass thresholds.

In Table IV we show the $J = 1/2$ and $J = 3/2$ dynamically-generated states ordered by increasing mass.

In the first and second columns we present the masses and widths of these states. The next column displays the (modulus of the) couplings to the different dominant baryon-meson channels, ordered by the threshold energies. The fourth column indicates the spin of the resonance while in the last column we show the baryon-meson channels that are allowed for decay.

Results on the Λ_b and Λ_b^* sectors have been previously discussed in Ref. [10]. However, in this latter work only the states coming from the most attractive SU(8) representations, the **120** and **168** irrep, were considered while the weakly attractive **4572** was disregarded. Moreover, the focus of this previous paper was the study of the recently discovered $\Lambda_b(5912)$ and $\Lambda_b(5920)$ states [28]. In the present paper we aim at studying the $\bar{B}N$ and $\bar{B}\Delta$ interactions to analyze the corresponding scattering amplitudes and, hence, the cross sections for the \bar{B} propagation in matter. Therefore, we analyze all resonant states appearing in the scattering amplitude stemming from all attractive representations for energies ranging from 5.8 GeV (close to the newly discovered states) up to 6.5 GeV.

We note that to achieve a better description of the $\Lambda_b(5912)$ and $\Lambda_b(5920)$ states reported by the LHCb Collaboration, we have slightly changed the value of the subtraction point used in the renormalization scheme [10],

$$\mu^2 = \alpha (M_{\Sigma_b}^2 + m_\pi^2), \quad (8)$$

with $\alpha = 0.967$. We will use the same value α in all sectors.

We observe that several of the $I = 0, J = 1/2$ states are very close in energy to the $I = 0, J = 3/2$ ones. In particular, some of these $J = 1/2$ and $J = 3/2$ states form HQSS doublets, as previously defined. As a formal rule, states with different spin and equal SU(6) and SU(3) labels form a HQSS multiplet [10, 16, 17]. We are considering the resonances stemming from the **120** and **168** SU(8) most attractive representations as well as the **4752** SU(8) irrep, this last one with a much higher multiplicity. Thus, the analysis of the adiabatic evolution of the states from the SU(6) \times HQSS symmetric point to the physical one in order to assign distinct SU(6) and SU(3) labels (in similar way as done in Refs. [10, 16, 17] for the states in the **120** and **168** irreps) is a much more tedious and difficult task, and is beyond the scope of the present paper. We have, however, restored HQSS in some cases, when the identifica-

M_R (MeV)	Γ_R (MeV)	Couplings to main channels	J	Open channels
5797.6	0.0	$g_{N\bar{B}} = 4.9, g_{N\bar{B}^*} = 8.3, g_{\Lambda\bar{B}_s^0} = 2.1, g_{\Lambda\bar{B}_s^*} = 3.6$	1/2	
5910.1	0.0	$g_{\Sigma_b\pi} = 1.8, g_{N\bar{B}} = 4.6, g_{N\bar{B}^*} = 3.0, g_{\Lambda_b\omega} = 1.4$	1/2	
5921.5	0.0	$g_{\Sigma_b^*\pi} = 1.8, g_{N\bar{B}^*} = 5.7, g_{\Lambda_b\omega} = 1.5$	3/2	
6009.3	0.0	$g_{\Lambda_b\eta} = 2.0, g_{N\bar{B}^*} = 1.7, g_{\Lambda\bar{B}_s^0} = 3.9, g_{\Lambda\bar{B}_s^*} = 6.0$	1/2	$\Sigma_b\pi$
6034.0	4.7	$g_{N\bar{B}} = 3.2, g_{N\bar{B}^*} = 2.2, g_{\Sigma_b\rho} = 2.2, g_{\Sigma_b^*\rho} = 1.4$	1/2	$\Sigma_b\pi$
6044.8	4.0	$g_{N\bar{B}^*} = 4., g_{\Lambda\bar{B}_s^*} = 1.3, g_{\Sigma_b\rho} = 1.1, g_{\Sigma_b^*\rho} = 2.4$	3/2	$\Sigma_b^*\pi$
6090.8	0.0	$g_{N\bar{B}^*} = 1., g_{\Xi_b K} = 2., g_{\Lambda\bar{B}_s^*} = 1.2, g_{\Sigma_b^*\rho} = 1.2$	1/2	$\Sigma_b\pi$
6094.1	2.6	$g_{\Xi_b' K} = 1.7, g_{\Lambda\bar{B}_s^0} = 5.7, g_{\Lambda\bar{B}_s^*} = 3.8, g_{\Lambda_b\phi} = 1.4$	1/2	$\Sigma_b\pi$
6105.4	2.5	$g_{\Xi_b^* K} = 1.7, g_{\Lambda\bar{B}_s^*} = 7.1, g_{\Lambda_b\phi} = 1.4, g_{\Xi_b^* K^*} = 1.6$	3/2	$\Sigma_b^*\pi$
6201.9	54.3	$g_{\Lambda_b\omega} = 2.2, g_{\Lambda\bar{B}_s^0} = 0.7, g_{\Sigma_b\rho} = 1.1, g_{\Xi_b' K^*} = 0.7$	1/2	$\Sigma_b\pi, \Lambda_b\eta$
6207.5	54.2	$g_{\Lambda_b\omega} = 2.2, g_{\Lambda\bar{B}_s^*} = 0.9, g_{\Sigma_b^*\rho} = 1.1, g_{\Xi_b^* K^*} = 0.8$	3/2	$\Sigma_b^*\pi$
6243.4	19.5	$g_{\Xi_b K} = 1.0, g_{\Sigma_b\rho} = 1.4, g_{\Sigma_b^*\rho} = 2.1$	1/2	$\Sigma_b\pi, \Lambda_b\eta, N\bar{B}$
6361.9	0.1	$g_{\Xi_b' K} = 1.6, g_{\Lambda_b\phi} = 1.5$	1/2	$\Sigma_b\pi, \Lambda_b\eta$
6373.3	0.1	$g_{\Xi_b^* K} = 1.6, g_{\Lambda\bar{B}_s^*} = 1.0, g_{\Lambda_b\phi} = 1.5$	3/2	$N\bar{B}, N\bar{B}^*, \Xi_b K$
6403.9	45.9	$g_{\Xi_b K} = 0.7, g_{\Xi_b' K^*} = 1.8, g_{\Xi_b^* K^*} = 2.4$	1/2	$\Sigma_b^*\pi, N\bar{B}^*$
6459.0	0.06	$g_{\Sigma_b\rho} = 2.3, g_{\Sigma_b^*\rho} = 1.0$	3/2	$\Sigma_b\pi, \Lambda_b\eta, N\bar{B}$
6463.8	1.6	$g_{\Lambda_b\phi} = 1.6, g_{\Xi_b K^*} = 2.3$	1/2	$N\bar{B}^*, \Xi_b K, \Lambda_b\omega$
6464.4	1.4	$g_{\Lambda_b\phi} = 1.5, g_{\Xi_b K^*} = 2.3$	3/2	$\Sigma_b^*\pi, N\bar{B}^*$
6515.6	6.1	$g_{\Lambda_b\phi} = 1.1, g_{\Xi_b' K^*} = 1.8, g_{\Xi_b^* K^*} = 1.4$	1/2	$\Lambda_b\omega, \Xi_b^* K$
6520.2	6.2	$g_{\Lambda_b\phi} = 1.0, g_{\Xi_b' K^*} = 1.1, g_{\Xi_b^* K^*} = 2.1$	3/2	$\Sigma_b\pi, \Lambda_b\eta, N\bar{B}, N\bar{B}^*$
6590.7	0.02	$g_{\Xi_b' K^*} = 2.5, g_{\Xi_b^* K^*} = 1.3$	3/2	$\Xi_b K, \Lambda_b\omega, \Xi_b' K, \Lambda\bar{B}_s^0$
				$\Sigma_b^*\pi, N\bar{B}^*$
				$\Lambda_b\omega, \Xi_b^* K$
				$\Sigma_b^*\pi, N\bar{B}^*, \Lambda_b\omega$
				$\Xi_b^* K, \Lambda\bar{B}_s^*, \Sigma_b\rho$

TABLE IV: Masses, widths and the most important couplings of the Λ_b and Λ_b^* baryon resonances ($I = 0; J = 1/2, J = 3/2$). In the first and second column we present the mass and width of these states. The next column displays the (modulus of the) dominant couplings to the different baryon-meson channels, ordered by the threshold energies. The fourth column indicates the spin of the resonance whereas in the last column we show the baryon-meson channels that are allowed for decay.

tion was dubious. We find seven HQSS doublets. While the HQSS doublet [$\Lambda_b(5910), \Lambda_b^*(5921)$] was discussed in Ref. [16] and assigned to the newly discovered $J = 1/2$ $\Lambda_b(5912)$ and $J = 3/2$ $\Lambda_b^*(5920)$ states [28], other HQSS doublets are: [$\Lambda_b(6034), \Lambda_b^*(6045)$], [$\Lambda_b(6094), \Lambda_b^*(6105)$], [$\Lambda_b(6202), \Lambda_b^*(6207)$], [$\Lambda_b(6362), \Lambda_b^*(6373)$], [$\Lambda_b(6464), \Lambda_b^*(6464)$] and [$\Lambda_b(6516), \Lambda_b^*(6520)$].

Several works have conjectured the existence of bottom baryonic resonances [29–34], most of them based on quark models. Recently baryon-meson calculations in the bottom sector using an extended hidden-gauge model have been carried out [35]. This work considers the interaction of $N\bar{B}, \Delta\bar{B}, N\bar{B}^*$ and $\Delta\bar{B}^*$ states with their coupled channels. The connection between \bar{B} and \bar{B}^* states with nucleon and Δ baryons is performed by requiring pion exchange, or anomalous terms, which are subleading in the large heavy-quark mass counting. The dynamics of the interaction is, though, different in our approach. In our model we consider simultaneously all baryon-pseudoscalar meson (BP) and

baryon-vector meson (BV) channels, with $J^P = 1/2^+$ and $3/2^+$ baryons, using a WT type-interaction that respects $SU(6) \times \text{HQSS}$ symmetry. The potential in the $BP - BP$ and $BV - BV$ sectors in both models is similar although a larger coupled-channel space is considered within our scheme. Moreover, the model of Ref. [35] uses a different renormalization scheme and takes into account a suppression factor in those transitions that involve a t -channel exchange of a heavy charm vector meson, which is not required from HQSS [10].

In Ref. [35], six Λ_b and Λ_b^* have been found, two of them associated to the experimental $\Lambda_b(5910)$ and $\Lambda_b^*(5921)$ states with an important coupling to \bar{B}^*N . Moreover, their $\Lambda_b(5821)$, with a strong coupling to $\bar{B}N$, was identified with our $\Lambda_b(5798)$ and the $\Lambda_b(5969)$ with a dominant coupling to $\Sigma_b\pi$ was assigned to our $\Lambda_b(6009)$. However, this last assignment seems dubious, since our $\Lambda_b(6009)$ does not couple strongly to $\Sigma_b\pi$. The two last states $\Lambda_b(6317)$ and $\Lambda_b^*(6316)$ in Ref. [35] couple strongly to $\Sigma_b\rho$. We could assign them to our HQSS doublet

$[\Lambda_b(6202), \Lambda_b^*(6207)]$ since we find an important coupling to $\Sigma_{b\rho}$ and $\Sigma_b^*\rho$, respectively, although our masses are smaller by 100 MeV and the widths are larger. Also, one could assign the $\Lambda_b(6317)$ of Ref. [35] to our $\Lambda_b(6243)$, due to the dominant $\Sigma_b^*\rho$ and $\Sigma_{b\rho}$ channels. The enlarged coupled-channel space in our model allows for a different composition of the resonant states as compared to the extended hidden-gauge scheme, thus making sometimes difficult a straightforward identification of the states between the two models.

2. Σ_b and Σ_b^* states ($I = 1; J = 1/2, 3/2$)

In the Σ_b sector, there are 22 channels

$$\begin{array}{cccccccc} \Lambda_b\pi & \Sigma_b\pi & N\bar{B} & N\bar{B}^* & \Xi_b K & \Sigma_b\eta & \Lambda_b\rho & \Xi_b' K \\ \Delta\bar{B}^* & \Sigma\bar{B}_s & \Sigma_b\rho & \Sigma_b\omega & \Sigma\bar{B}_s^* & \Sigma_b^*\rho & \Sigma_b^*\omega & \Xi_b K^* \\ \Sigma_b\eta' & \Sigma^*\bar{B}_s & \Xi_b' K^* & \Sigma_b\phi & \Xi_b^* K^* & \Sigma_b^*\phi & & \end{array}$$

In the Σ_b^* sector, we find 20 channels

$$\begin{array}{cccccccc} \Sigma_b^*\pi & N\bar{B}^* & \Sigma_b^*\eta & \Lambda_b\rho & \Xi_b^* K & \Delta\bar{B} & \Delta\bar{B}^* & \Sigma_b\rho \\ \Sigma_b\omega & \Sigma\bar{B}_s^* & \Sigma_b^*\rho & \Sigma_b^*\omega & \Xi_b K^* & \Sigma^*\bar{B}_s & \Sigma_b^*\eta' & \Sigma^*\bar{B}_s^* \\ \Xi_b^* K^* & \Sigma_b\phi & \Xi_b^* K^* & \Sigma_b^*\phi & & & & \end{array}$$

In both cases the channels are ordered by increasing mass thresholds.

We show in Table V several $J = 1/2$ and $J = 3/2$ states ordered by increasing mass, in a similar way as done in Table IV. As described in the Λ_b and Λ_b^* sectors, we can also distinguish several HQSS doublets due to their decay modes and closeness in mass. We find eight HQSS doublets, such as $[\Sigma_b(5812), \Sigma_b^*(5820)]$, $[\Sigma_b(5971), \Sigma_b^*(5980)]$, $[\Sigma_b(6021), \Sigma_b^*(6028)]$, $[\Sigma_b(6217), \Sigma_b^*(6228)]$, $[\Sigma_b(6309), \Sigma_b^*(6319)]$, $[\Sigma_b(6359), \Sigma_b^*(6365)]$, $[\Sigma_b(6469), \Sigma_b^*(6479)]$ and $[\Sigma_b(6512), \Sigma_b^*(6517)]$.

It is also interesting to note that our state $\Sigma_b(5904)$ can be interpreted as the counterpart of the $\Sigma^*(1670)$ and $\Sigma_c^*(2549)$ in the strange and charm sectors, respectively. This assignment is due to the fact that this state has a dominant $\Delta\bar{B}$ component, in a similar manner as the $\Sigma^*(1670)$ and $\Sigma_c^*(2549)$ resonances strongly couple to $\Delta\bar{K}$ and ΔD , respectively. This state has not been found experimentally yet, but it is a clear case for discovery.

As also mentioned for the Λ_b and Λ_b^* , the straightforward comparison with the predicted Σ_b and Σ_b^* states of Ref. [35] is difficult in some cases. However, in Ref. [35], the bottom counterpart of the $\Sigma^*(1670)$ and $\Sigma_c^*(2549)$ could be traced to the $\Sigma_b^*(5933)$, 30 MeV above our prediction. Moreover, our HQSS doublet $[\Sigma_b(6021), \Sigma_b^*(6028)]$ could be identified with $\Sigma_b(6023)$ of Ref. [35]. This state, however, couples most strongly to $\bar{B}^*\Delta$ while the $\Sigma_b(6021)$ couples dominantly to $\Sigma\bar{B}_s$ and the $\Sigma_b^*(6028)$ resonance couples strongly to $\Sigma\bar{B}_s^*$. These two-particle channels are not present in the coupled-channel space of Ref. [35], since states with strangeness and hidden strangeness are not taken into account.

3. ($I = 2; J = 3/2$) states

In this sector we have 5 channels

$$\Sigma_b^*\pi \quad \Delta\bar{B} \quad \Delta\bar{B}^* \quad \Sigma_b\rho \quad \Sigma_b^*\rho$$

again ordered by increasing mass thresholds.

As seen in Table VI, we obtain three resonances with masses 5909 MeV, 6049 MeV and 6395 MeV. Whereas the first two states are mainly formed by $\Delta\bar{B}$ and $\Delta\bar{B}^*$, the last one mostly couples to $\Sigma_b^*\rho$. In Ref. [35] it was indicated that the $I = 2$ sector is repulsive and, thus, no dynamically-generated states can be found. However, in this previous work the $\Sigma_b\rho$ and $\Sigma_b^*\rho$ channels were not considered in the coupled basis. In our model, the inclusion of these two channels provides some attraction and allows for the formation of the three dynamically-generated baryon-meson states.

III. \bar{B} MESON PROPAGATION IN HADRONIC MATTER

In the last section we have obtained a realistic description of the interactions of a \bar{B} meson with light mesons and baryons, by means of unitarized effective field theories. An immediate application is to study the \bar{B} meson propagation in a dense and hot medium composed of lighter mesons and baryons.

If a hadron mixture –such as a hadron gas in heavy-ion collisions– is out of equilibrium, the scattering of a heavy meson with other species implies momentum loss as well as entropy production. These effects are encoded into the transport coefficients of heavy mesons and, in particular, in the medium drag force and the diffusion coefficients [36].

In a collective description, the distribution function of \bar{B} mesons, $f(t, \mathbf{p})$, obeys a Boltzmann-like transport equation, provided that the system is dilute enough and there are no correlations between collisions. In this picture, the heavy meson behaves as a Brownian particle suffering from collisions with the bath's particles. In the limit of a large Brownian mass (in comparison to the other masses), the transport equation can be recasted into a Fokker-Planck equation:

$$\frac{\partial f(t, \mathbf{p})}{\partial t} = \frac{\partial}{\partial p_i} \left\{ F_i(\mathbf{p}) f(t, \mathbf{p}) + \frac{\partial}{\partial p_j} [\Gamma_{ij}(\mathbf{p}) f(t, \mathbf{p})] \right\}, \quad (9)$$

with $i, j = 1, 2, 3$ the spatial indices. The quantity F_i is the drag force, which is a function of the heavy-meson momentum,

$$F_i(\mathbf{p}) = \int d\mathbf{k} w(\mathbf{p}, \mathbf{k}) k_i, \quad (10)$$

and Γ_{ij} is the momentum diffusion matrix [5, 36],

$$\Gamma_{ij}(\mathbf{p}) = \frac{1}{2} \int d\mathbf{k} w(\mathbf{p}, \mathbf{k}) k_i k_j. \quad (11)$$

M_R (MeV)	Γ_R (MeV)	Couplings to main channels	J	Open channels
5811.8	0.1	$g_{\Sigma_b\pi} = 2., g_{N\bar{B}} = 5.7, g_{N\bar{B}^*} = 3.7, g_{\Delta\bar{B}^*} = 2.8$	1/2	$\Lambda_b\pi$
5820.4	0.0	$g_{\Sigma_b^*\pi} = 1.9, g_{N\bar{B}^*} = 6.9, g_{\Delta\bar{B}} = 1.8, g_{\Delta\bar{B}^*} = 2.1$	3/2	
5903.6	0.0	$g_{\Delta\bar{B}} = 6., g_{\Delta\bar{B}^*} = 4.5, g_{\Sigma_b\omega} = 2.7$	3/2	
5909.3	0.0	$g_{N\bar{B}^*} = 2.3, g_{\Sigma_b^*\eta} = 2.2, g_{\Delta\bar{B}^*} = 2.3, g_{\Sigma^*\bar{B}_s} = 4.5, g_{\Sigma^*\bar{B}_s^*} = 5.5$	3/2	
5911.0	0.0	$g_{N\bar{B}} = 1.8, g_{\Sigma_b\eta} = 2.2, g_{\Xi'_b K} = 1.8, g_{\Sigma\bar{B}_s} = 2.8, g_{\Sigma^*\bar{B}_s^*} = 7.1$	1/2	$\Lambda_b\pi$
5918.4	0.0	$g_{\Xi_b K} = 2.6, g_{\Sigma\bar{B}_s} = 3.7, g_{\Sigma\bar{B}_s^*} = 6.2, g_{\Sigma^*\bar{B}_s^*} = 1.8$	1/2	$\Lambda_b\pi$
5970.6	0.5	$g_{\Xi'_b K} = 2.1, g_{\Sigma\bar{B}_s} = 5.5, g_{\Sigma\bar{B}_s^*} = 3.8, g_{\Sigma^*\bar{B}_s^*} = 2.7$	1/2	$\Lambda_b\pi, \Sigma_b\pi$
5980.4	0.4	$g_{\Xi_b^* K} = 1.9, g_{\Sigma\bar{B}_s^*} = 7., g_{\Xi_b K^*} = 1.8, g_{\Sigma^*\bar{B}_s^*} = 1.7$	3/2	$\Sigma_b^*\pi$
6015.0	2.6	$g_{N\bar{B}^*} = 1.8, g_{\Sigma_b\rho} = 1.7, g_{\Sigma_b^*\rho} = 1.9, g_{\Sigma\bar{B}_s^*} = 3.$	1/2	$\Lambda_b\pi, \Sigma_b\pi$
6020.6	10.0	$g_{\Lambda_b\rho} = 1.6, g_{\Sigma\bar{B}_s} = 2.2, g_{\Delta\bar{B}^*} = 2., g_{\Xi_b K^*} = 1.4$	1/2	$\Lambda_b\pi, \Sigma_b\pi$
6027.6	9.1	$g_{\Lambda_b\rho} = 1.6, g_{\Delta\bar{B}^*} = 1.6, g_{\Sigma\bar{B}_s^*} = 2.3, g_{\Xi_b K^*} = 1.4$	3/2	$\Sigma_b^*\pi$
6051.4	0.02	$g_{\Sigma^*\bar{B}_s} = 5.7, g_{\Xi'_b K^*} = 2.7, g_{\Sigma_b\phi} = 1.8, g_{\Sigma^*\bar{B}_s^*} = 5.$	3/2	$\Sigma_b^*\pi$
6216.7	38.0	$g_{\Sigma_b\eta} = 1., g_{\Sigma_b\omega} = 1.5, g_{\Sigma_b^*\omega} = 0.8, g_{\Xi_b K^*} = 1.1$	1/2	$\Lambda_b\pi, \Sigma_b\pi$
6227.9	38.1	$g_{\Sigma_b^*\pi} = 0.8, g_{\Lambda_b\rho} = 0.8, g_{\Sigma_b^*\eta} = 1., g_{\Sigma_b^*\omega} = 1.6, g_{\Xi_b K^*} = 1.1$	3/2	$\Sigma_b^*\pi$
6256.0	41.4	$g_{\Lambda_b\pi} = 0.7, g_{\Sigma_b\omega} = 1.5, g_{\Sigma_b^*\omega} = 2.2$	1/2	$\Lambda_b\pi, \Sigma_b\pi, N\bar{B}$
6308.8	6.6	$g_{\Sigma_b\eta} = 0.9, g_{\Sigma_b\omega} = 1.6, g_{\Sigma_b^*\omega} = 1.3, g_{\Xi_b K^*} = 1.$	1/2	$\Lambda_b\pi, \Sigma_b\pi, N\bar{B}$ $N\bar{B}^*, \Xi_b K$
6319.0	6.1	$g_{\Sigma_b^*\eta} = 1., g_{\Sigma_b^*\omega} = 1.8, g_{\Xi_b K^*} = 1.$	3/2	$\Sigma_b^*\pi, N\bar{B}^*$
6359.3	0.2	$g_{\Lambda_b\rho} = 1., g_{\Sigma_b\rho} = 1.7, g_{\Sigma_b^*\rho} = 1.2$	1/2	$\Lambda_b\pi, \Sigma_b\pi, N\bar{B}, N\bar{B}^*$
6364.7	0.1	$g_{\Lambda_b\rho} = 1., g_{\Sigma_b\rho} = 1.1, g_{\Sigma_b^*\rho} = 1.8$	3/2	$\Sigma_b^*\pi, N\bar{B}$
6401.7	28.7	$g_{\Sigma\bar{B}_s^*} = 1., g_{\Sigma_b\phi} = 1.3, g_{\Sigma_b^*\phi} = 1.8, g_{\Xi_b^* K^*} = 1.2$	1/2	$\Lambda_b\pi, \Sigma_b\pi, N\bar{B},$ $N\bar{B}^*, \Xi_b K, \Sigma_b\eta, \Lambda_b\rho$
6409.8	0.1	$g_{\Sigma_b\rho} = 1.9, g_{\Sigma_b\omega} = 1.2, g_{\Sigma_b^*\rho} = 1.1$	3/2	$\Sigma_b^*\pi, N\bar{B}^*, \Lambda_b\rho, \Sigma_b^*\eta$
6469.2	16.4	$g_{\Xi'_b K^*} = 1.9, g_{\Sigma_b\phi} = 1.5, g_{\Xi_b^* K^*} = 1.1$	1/2	$\Lambda_b\pi, \Sigma_b\pi, N\bar{B}, N\bar{B}^*$ $\Xi_b K, \Sigma_b\eta, \Lambda_b\rho, \Xi'_b K$
6478.6	15.1	$g_{\Xi'_b K^*} = 0.9, g_{\Sigma_b^*\phi} = 1.5, g_{\Xi_b^* K^*} = 2.$	3/2	$\Sigma_b^*\pi, N\bar{B}^*, \Lambda_b\rho$ $\Sigma_b^*\eta, \Delta\bar{B}, \Xi_b^* K$
6512.5	0.6	$g_{\Xi_b K^*} = 1.4, g_{\Xi'_b K^*} = 1., g_{\Sigma_b\phi} = 1.7, g_{\Sigma_b^*\phi} = 1.2$	1/2	$\Lambda_b\pi, \Sigma_b\pi, N\bar{B}$
6517.0	0.6	$g_{\Xi_b K^*} = 1.4, g_{\Sigma_b\phi} = 1.2, g_{\Sigma_b^*\phi} = 1.8, g_{\Xi_b^* K^*} = 1.1$	3/2	$N\bar{B}^*, \Xi_b K, \Sigma_b\eta, \Lambda_b\rho$ $\Sigma_b^*\pi, N\bar{B}^*, \Lambda_b\rho$
6542.2	1.4	$g_{\Xi'_b K^*} = 1., g_{\Sigma_b\phi} = 0.9, g_{\Sigma_b^*\phi} = 1.6, g_{\Xi_b^* K^*} = 1.7$	1/2	$\Sigma_b^*\eta, \Delta\bar{B}, \Xi_b^* K$ $\Lambda_b\pi, \Sigma_b\pi, N\bar{B}, N\bar{B}^*$
6549.0	0.02	$g_{\Xi'_b K^*} = 1.4, g_{\Sigma_b\phi} = 2., g_{\Sigma_b^*\phi} = 1.3$	3/2	$\Xi_b K, \Sigma_b\eta, \Lambda_b\rho, \Xi'_b K$ $\Sigma_b^*\pi, N\bar{B}^*, \Lambda_b\rho$ $\Sigma_b^*\eta, \Delta\bar{B}, \Xi_b^* K, \Delta\bar{B}^*$

TABLE V: As in Table IV, but for Σ_b and Σ_b^* baryon resonances ($I = 1; J = 1/2, J = 3/2$).

M_R (MeV)	Γ_R (MeV)	Couplings to main channels	J	Open channels
5907.8	0.0	$g_{\Sigma_b^*\pi} = 2.2, g_{\Delta\bar{B}} = 4.8, g_{\Delta\bar{B}^*} = 5.9$	3/2	
6048.6	0.05	$g_{\Delta\bar{B}} = 5.4, g_{\Delta\bar{B}^*} = 4.6, g_{\Sigma_b\rho} = 2.8, g_{\Sigma_b^*\rho} = 1.3$	3/2	$\Sigma_b^*\pi$
6395.1	31.1	$g_{\Sigma_b\rho} = 1.1, g_{\Sigma_b^*\rho} = 2.5$	3/2	$\Sigma_b^*\pi$

TABLE VI: As in Table IV, but for baryon resonances in the $I = 2; J = 3/2$ sector.

The collision rate $w(\mathbf{p}, \mathbf{k})$ is a remnant of the collision integral in the Boltzmann equation. It reads

$$\begin{aligned}
w(\mathbf{p}, \mathbf{k}) &= g_l \int \frac{d^3q}{(2\pi)^9} n_{F,B}(E_l(q), T) [1 \pm n_{F,B}(E_l(q+k), T)] \frac{1}{2E_{\bar{B}}(p)} \frac{1}{2E_l(q)} \frac{1}{2E_{\bar{B}}(p-k)} \frac{1}{2E_l(q+k)} \\
&\times (2\pi)^4 \delta(E_{\bar{B}}(p) + E_l(q) - E_{\bar{B}}(p-k) - E_l(q+k)) |\mathcal{M}^2|, \tag{12}
\end{aligned}$$

where \bar{B} represents the bottom meson and l the light hadron of the thermal bath. The quantity g_l stands for the spin-isospin degeneracy factor of the light hadron and $n_{F,B}(E_l, T)$ is the light hadron equilibrium distribution function that follows Fermi-Dirac or Bose-Einstein statistics. The invariant scattering matrix element is given by \mathcal{M} . This is computed as

$$\mathcal{M}_{ij}(\sqrt{s}) = \gamma_i^{1/2} \gamma_j^{1/2} T_{ij}(\sqrt{s}) , \quad (13)$$

once the scattering amplitude T_{ij} of Eq. (1) is known, with $\gamma_i = 1$ for meson-meson scattering and $\gamma_i = 2M_i$, with M_i the mass of the baryon, for baryon-meson scattering.

Assuming an isotropic bath, the transport coefficients $F_i(\mathbf{p})$ and $\Gamma_{ij}(\mathbf{p})$ can be written as

$$F_i(\mathbf{p}) = F(p) p_i , \quad (14)$$

$$\Gamma_{ij}(\mathbf{p}) = \Gamma_0(p) \left(\delta_{ij} - \frac{p_i p_j}{p^2} \right) + \Gamma_1(p) \frac{p_i p_j}{p^2} , \quad (15)$$

in terms of three scalar functions, $F(p)$, $\Gamma_0(p)$ and $\Gamma_1(p)$, given by

$$F(p) = \int d\mathbf{k} w(\mathbf{p}, \mathbf{k}) \frac{k_i p^i}{p^2} , \quad (16)$$

$$\Gamma_0(p) = \frac{1}{4} \int d\mathbf{k} w(\mathbf{p}, \mathbf{k}) \left[\mathbf{k}^2 - \frac{(k_i p^i)^2}{p^2} \right] , \quad (17)$$

$$\Gamma_1(p) = \frac{1}{2} \int d\mathbf{k} w(\mathbf{p}, \mathbf{k}) \frac{(k_i p^i)^2}{p^2} . \quad (18)$$

In the so-called *static limit* (where the \bar{B} -meson momentum goes to zero) only one of the three coefficients is independent. On one hand, the two diffusion coefficients become degenerate,

$$\lim_{p \rightarrow 0} [\Gamma_0(p) - \Gamma_1(p)] = 0 . \quad (19)$$

On the other hand, the Einstein relation relates F with $\Gamma = \Gamma_0 = \Gamma_1$ as

$$\lim_{p \rightarrow 0} F(p) = \frac{\Gamma(p)}{m_B T} . \quad (20)$$

Apart from the transport coefficients, there exist other quantities of interest. The relaxation time τ_R is defined as the inverse of the drag force:

$$\tau_R = \frac{1}{F} , \quad (21)$$

and corresponds to the characteristic time of relaxation for the momentum distribution [7]. Moreover, the spatial diffusion coefficient (defined in the static limit)

$$D_x = \lim_{p \rightarrow 0} \frac{\Gamma(p)}{m_B^2 F^2(p)} , \quad (22)$$

measures the homogenization speed of bottom mesons in the position space [7] (q.v. [36] on diffusion phenomena).

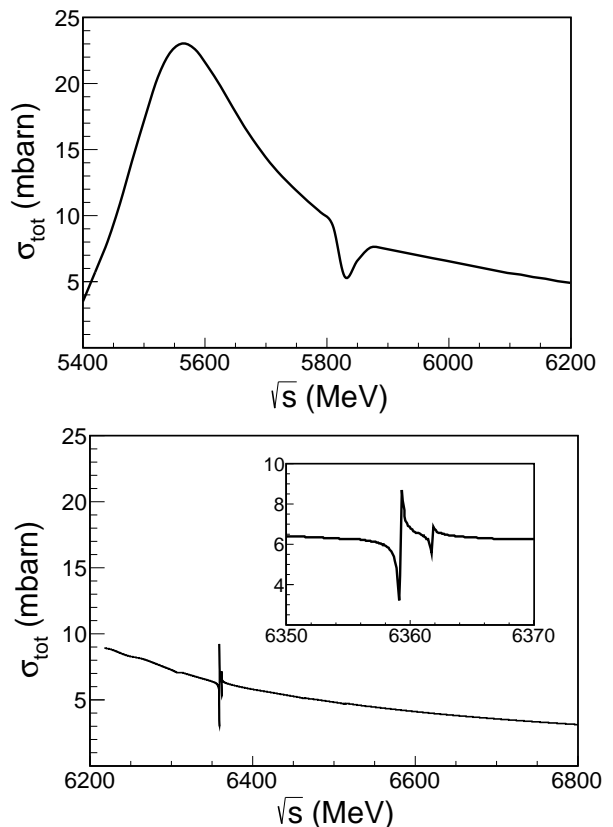


FIG. 1: Upper panel: $\bar{B}\pi$ isospin averaged total cross section as a function of the C.M. energy. Lower panel: same for the $N\bar{B}$ scattering.

A. Transport coefficients of \bar{B} mesons

In this section we present our results on the transport coefficients for a \bar{B} meson. As opposed to the charmed analogue in Ref. [6] we restrict ourselves to the case of nearly vanishing baryochemical potential. This is due to the fact that the large mass of \bar{B} mesons makes unlikely their production in colliders such as FAIR or NICA [37], where the finite- μ_B part of the Quantum Chromodynamics (QCD) phase diagram will be explored. Only for high-energy colliders such as RHIC or LHC, there is enough initial energy to produce \bar{B} mesons.

The magnitude of the coefficients in Eqs. (16,17,18) is roughly determined by the product of the density of light particles and the collision rate (see also Eq. (24) for a nonrelativistic estimate in kinetic theory). Therefore, the cross section represents a fundamental piece in the computation of the drag force and diffusion coefficients. Thus, the presence of resonant structures, as those described in Secs. II A and II B, will strongly affect the final values of the transport coefficients.

In Fig. 1 we plot the $\bar{B}\pi$ and $N\bar{B}$ elastic cross sections. These are the dominant cross sections due to a major abundance of pions (nucleons) with respect to the other species in the meson (baryon) sectors.

In the upper panel, we show the isospin averaged elastic cross section for $\bar{B}\pi$ scattering. This cross section can be compared to our previous computation in Ref. [9]. As seen in [9], we find that the cross section is dominated by the presence of the B_0 resonance at $\sqrt{s} = 5530$ MeV. There exist, however, two clear differences between our current calculation and the previous one. First, the overall magnitude of the current cross section is slightly smaller than that in our previous reference. This is related to new choice of low-energy constants h_3, h_5 and the subtraction constant. The second difference is the clear depression around $\sqrt{s} = 5830$ MeV. This feature corresponds to the opening of the $\bar{B}_s\bar{K}$ channel at $\sqrt{s} = 5862$ MeV as the resonance at 5827 MeV starts to form.

In the lower panel we display the isospin-averaged $N\bar{B}$ cross section. Note that the magnitude of the cross section is of the same order as the one for the pions away from the B_0 peak. The behavior of the cross section is quite smooth except in the energy region around $\sqrt{s} = 6360$ MeV, where the $I = 0$ 6361 MeV and the $I = 1$ 6359 MeV resonances appear. These states couple to $N\bar{B}$ having a very small width and, thus, the average cross section varies abruptly in a small energy domain.

The cross sections in Fig. 1 (to be precise, the squared scattering amplitudes) together with those for the \bar{B} mesons interacting with K, \bar{K}, η and Δ are needed to calculate the transport coefficients of Eqs. (16,17,18). We start by considering the zero baryochemical potential, $\mu_B = 0$ case, in order to compare with our previous work in Ref. [9]².

In the upper panel of Fig. 2 we show the drag force F as a function of temperature (T) at $\mu_B = 0$ and $p = 100$ MeV. Only the \bar{B} -light meson (π, K, \bar{K}, η) scattering has been taken into account in this case.

In spite of the addition of more channels in the unitarization procedure and the modification of the LECs and the subtraction point, the final result of the drag force is similar to the one in Ref. [9]. As seen in [9], the calculations of [8] differ from our results due to the simplified input used for the scattering amplitudes. We have also checked that the inclusion of the \bar{B} scattering with N and Δ makes no appreciable difference in the $\mu_B = 0$ case. As a matter of fact, the resulting curve lies on the top of the one presented here, making the baryonic contribution totally negligible. With regard to the diffusion coefficients in the static limit ($\Gamma_0 = \Gamma_1$), the Einstein relation provides them in terms of the drag force F .

In order to analyze the contribution of baryons to the transport coefficients, one has to increase the baryochemical potential. However, a large baryochemical potential

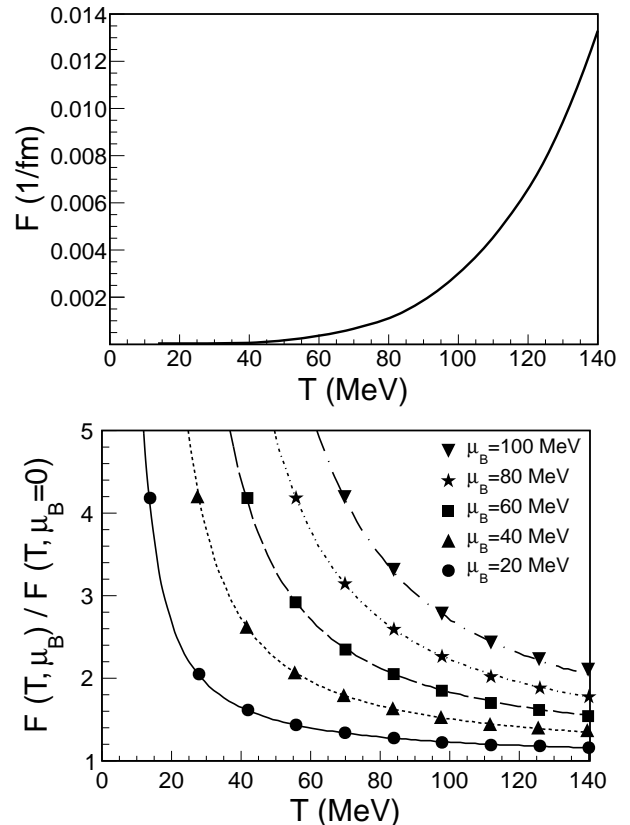


FIG. 2: Upper panel: Drag force of a \bar{B} meson in a bath of π, K, \bar{K} and η mesons. The baryon chemical potential is set to $\mu_B = 0$ and the momentum of the heavy meson to $p = 100$ MeV. Lower panel: Drag force coefficient as a function of temperature for several μ_B (normalized to the $\mu_B = 0$ case).

is of very limited interest as \bar{B} mesons are difficult to produce in low-energy heavy-ion collisions, where the finite μ_B regime of the QCD phase diagram is probed.

In the lower panel of Fig. 2 we plot the drag force at different baryochemical potentials for the same range of temperatures as the upper one and again at fixed $p = 100$ MeV. As the absolute value of this coefficient is negligible with respect to the contribution from mesons, we have decided to normalize it with respect to the $\mu_B = 0$ case. In this way, we can verify the simple relation,

$$F(T, \mu_B) = z(\mu_B) F(T, \mu_B = 0), \quad (23)$$

with $z = e^{\mu_B/T}$ being the fugacity [6]. The numerical results using Eq. (16) are shown with symbols for $\mu_B = 20, 40, 60, 80, 100$ MeV. On top of the computation, we have plotted the analytical function $e^{\mu_B/T}$ for the same values of the baryochemical potential. The agreement between the two is excellent, providing a numerical check of Eq. (23) (a similar expression also holds for the diffusion coefficient). Note that this expression is only valid for the pure baryonic contribution, still very small compared with the mesonic contribution for low temperatures (Boltzmann suppression) and low baryochemical potentials (small net baryonic density).

² The scattering amplitudes and, hence, cross sections might be modified in matter due to finite density and temperature effects. The study of these modifications is, however, left for future work in order to carry a detailed many-body calculation of the scattering amplitudes in matter. This effect is, in any case, subdominant.

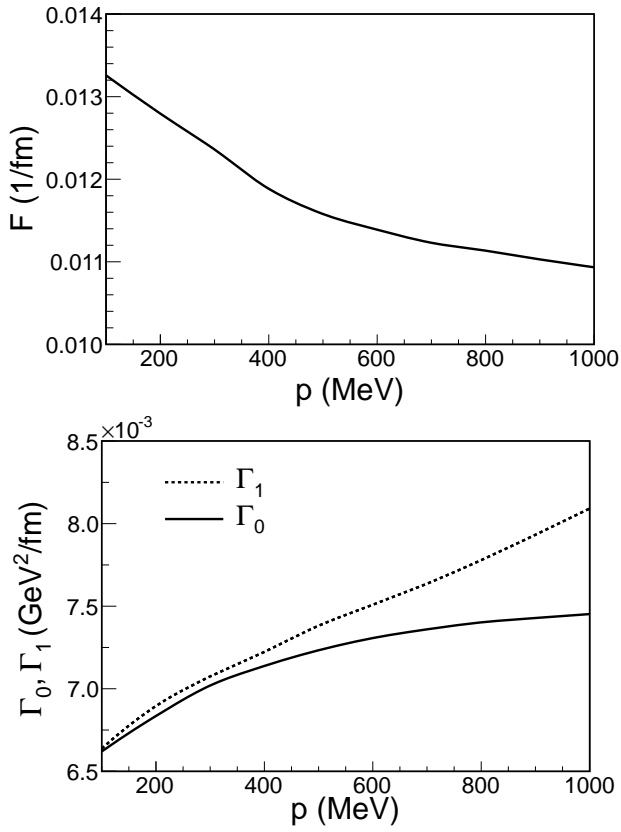


FIG. 3: Drag force and diffusion coefficients of a \bar{B} meson in a bath composed of π, K, \bar{K}, η mesons and N and Δ baryons. The baryon chemical potential is fixed at $\mu_B = 0$ and the temperature at $T = 140$ MeV. The heavy meson momentum runs from the static limit (taken at $p = 100$ MeV) to $p = 1$ GeV.

In what follows we will present our results of the transport coefficients including all species ($\pi, K, \bar{K}, \eta, N, \Delta$). First, we explore their momentum dependence at constant $\mu_B = 0$ and $T = 140$ MeV. The results for the three transport coefficients are shown in Fig. 3. In this case, the two diffusion coefficients are not degenerate anymore, although the fluctuation-dissipation theorem still relates the three transport coefficients [5, 36]. These results are compatible with the ones in Ref. [9], being our result systematically smaller because the temperature is now $T = 140$ MeV.

So far we have shown the transport coefficients that appear in the Fokker-Planck equation. These coefficients serve as inputs for the numerical propagation of the heavy meson in a hadronic environment based on Langevin dynamics [38, 39]. Alternatively, we present other quantities that possess a more physical insight. In particular, we pay attention to the relaxation time τ_R and the spatial diffusion coefficient D_x . These coefficients can be computed in terms of F , Γ_0 and Γ_1 , according to Eqs. (21,22). We concentrate on physical trajectories in the QCD phase diagram for the hadronic medium created at RHIC/LHC collisions, with a large entropy per baryon

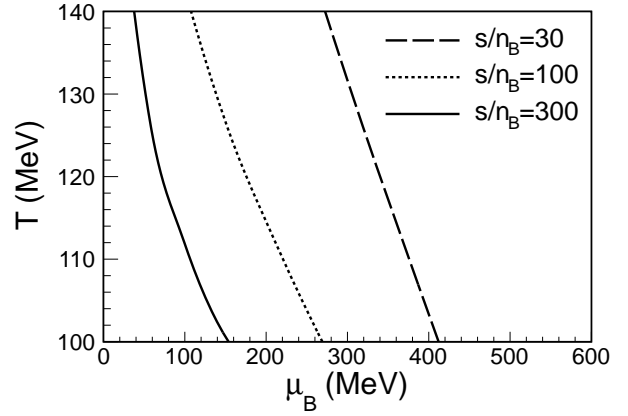


FIG. 4: Upper panel: Isentropic trajectories on the phase diagram for collisions at RHIC ($s/n_B = 100, 300$) and FAIR at its highest expected energy $s/n_B = 30$.

being constant. As a limiting case, we present results for a typical FAIR trajectory at its highest energy, with a fixed entropy per baryon around $s/n_B = 30$ [40, 41].

Three characteristic trajectories are shown in Fig. 4 for fixed entropy per baryon $s/n_B = 30, 100$ and 300 . The last two are the predicted values for collisions at RHIC [41]. At high T , the lines get closer to the $\mu_B = 0$ trajectory (thermal evolution of the early universe) as long as we increase the entropy per baryon. At low temperatures all the curves bend towards large μ_B .

In the upper panel of Fig. 5 we show the relaxation time $\tau_R = 1/F$. Because τ_R is much larger than the lifetime of the system [42, 43], the bottom can hardly relax during the fireball expansion. In other words, the collisions with other particles are not enough to appreciably reduce the average momentum. The three curves are quite similar in the whole range of temperatures. In fact, we have added the limiting case of $\mu_B = 0$ that corresponds to $s/n_B \rightarrow \infty$ and check that it is almost indistinguishable from the curve of $s/n_B = 100$. For collisions with larger baryonic density (lower entropy per baryon) the relaxation time is smaller, because the heavy meson scatters more, but not enough to represent an efficient mechanism of relaxation.

One can also compare these results to those for the charm case in Ref. [6]. The drag coefficient naively scales with the inverse mass of the heavy meson

$$F \sim P\sigma\sqrt{\frac{m_l}{T}}\frac{1}{m_B}, \quad (24)$$

where P is the pressure of the bath, σ is the total cross section and m_l is the mass of the bath's particles. Assuming comparable interactions (i.e. similar cross sections), we expect $\tau_R(\text{bottom})/\tau_R(\text{charm}) \sim m_B/m_D \simeq 2.8$. Comparing with the curve of $s/n_B = 30$ in Ref. [6], one can check that this is indeed satisfied (the breaking of this scaling can be accounted by differences in the cross sections). As a representative value for the bottom case we can quote a relaxation time of $\tau_R(\text{bottom}) = 67.9$ fm

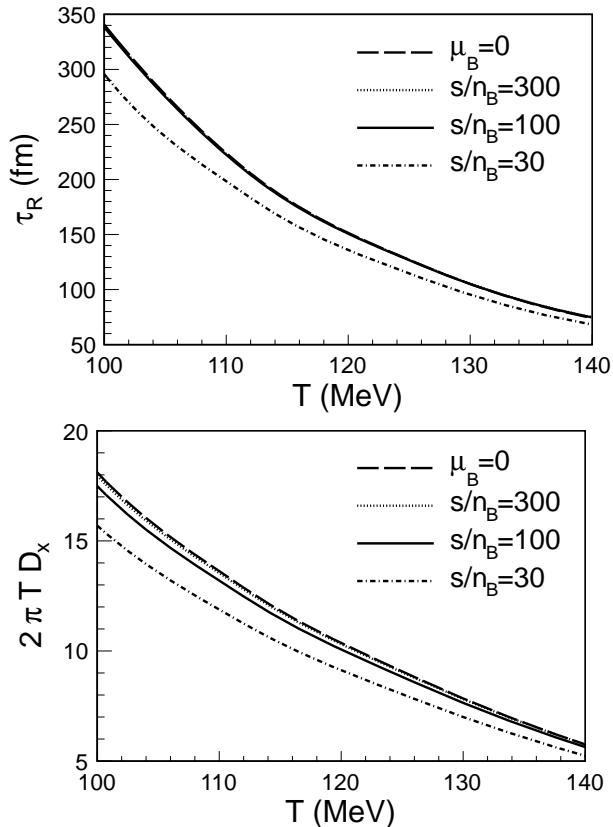


FIG. 5: Spatial diffusion coefficient multiplied by the thermal wavelength ($2\pi T$) for the different isentropic curves shown in Fig. 4.

for $T = 140$ MeV at $s/n_B = 30$. This value has to be compared with $\tau_R(\text{charm}) = 28.3$ fm at the same temperature and entropy per baryon [6].

Finally, in the lower panel of Fig. 5 we plot the spatial diffusion coefficient D_x . This coefficient is multiplied by the thermal wavelength ($2\pi T$) to form an adimensional number, like the Reynolds or the Knudsen numbers. The results are again quite independent of the entropy per baryon as long as the collision energy is high enough. In conclusion, our results can be taken as prediction for the hadronic medium created at high energy collisions (like those at the RHIC or the LHC) independently of the precise value of the entropy per baryon of the trajectory.

IV. CONCLUSIONS

We have studied the interaction and propagation of \bar{B} mesons in hadronic matter made of light mesons, N and Δ , by means of a unitarized approach based on effective models that are compatible with chiral and heavy quark symmetries.

We have examined the \bar{B} scattering with mesons and baryons by analyzing the dynamically generated states in the meson and baryon sectors where the \bar{B} meson and

its HQSS partner, the \bar{B}^* meson, are present. In the open bottom meson sector there is a strong resemblance between the 0^+ and 1^+ spectrum due to HQSS. Among others, we have found two non-strange resonances that form a HQSS doublet, the $B_0(5530)$ and $B_1(5579)$ states, which turn out to be the bottom counterparts of the experimental $D_0(2400)$ and $D_1(2430)$, respectively. These resonances have not been experimentally observed yet. Moreover, another doublet with strangeness, $B_{s0}^*(5748)$ and $B_{s1}^*(5799)$, can be identified as the bottom analogues of the $D_{s0}^*(2317)$ and the $D_{s1}(2460)$. For baryons we have also determined several $J = 1/2$ and $J = 3/2$ states in the Λ_b and Σ_b sectors which form HQSS doublets. This is the case of the $\Lambda_b(5910)$ and $\Lambda_b^*(5921)$, which can be identified with the states observed by the LHCb collaboration [28]. Furthermore, we have associated one of our states, the $J = 3/2$ $\Sigma_b^*(5904)$ to be the bottom counterpart of the strange $\Sigma^*(1670)$ and charmed $\Sigma_c^*(2549)$ resonances, though not experimentally detected yet but a clear case for discovery.

Next we have analyzed different transport coefficients that describe the propagation of \bar{B} mesons in hadronic matter. We have shown the drag and diffusion coefficients for vanishing baryochemical potential, which serve as inputs for the numerical propagation of the heavy meson in matter produced at high-energy colliders like RHIC or LHC. At $\mu_B = 0$ the main contribution to the drag and diffusion coefficients comes from the interaction of \bar{B} mesons with pions as the thermal bath is mainly populated by this species. Alternatively, we have also presented other quantities that possess a more physical insight, such as the relaxation time τ_R and the spatial diffusion coefficient D_x for isentropic trajectories within the QCD phase diagram. These trajectories range from the region explored by the RHIC and LHC experiments up to FAIR at its top energy. We have checked that the naive scaling of the relaxation time with the inverse mass of the heavy meson is fulfilled. Moreover, although the relaxation time is smaller with larger baryonic density, the \bar{B} meson can hardly relax to the equilibrium. Indeed, our results can be taken as predictions for the hadronic medium created at high energy collisions (like those at the RHIC or the LHC) independently of the precise value of the entropy per baryon of the trajectory as long as the collision energy is high enough.

Acknowledgments

We would like to thank L. Abreu for providing us with the coefficients of Table I. This work has been funded by Grants No. FPA2010-16963 (Ministerio de Ciencia e Innovación) and No. FP7-PEOPLE-2011-CIG under Contract No. PCIG09-GA-2011-291679. We acknowledge the support of the European Community-Research Infrastructure Integrating Activity Study of Strongly Interacting Matter (acronym HadronPhysics3, Grant Agreement n. 283286) under the Seventh Frame-

work Programme of EU. L.T. acknowledges support from the Ramón y Cajal Research Programme (Ministerio de Ciencia e Innovación). J.M.T.-R. is also supported by the Programme TOGETHER from Région Pays de la Loire

and the European I3-Hadron Physics programme.

-
- [1] B. Abelev *et al.* [ALICE Collaboration], Phys. Rev. Lett. **109**, 112301 (2012) [arXiv:1205.6443 [hep-ex]].
- [2] M. Laine, J. High energy Phys. **04**, 124 (2011) [arXiv:1103.0372 [hep-ph]].
- [3] M. He, R. J. Fries and R. Rapp, Phys. Lett. B **701**, 445 (2011) [arXiv:1103.6279 [nucl-th]].
- [4] S. Ghosh, S. K. Das, S. Sarkar and J. -eAlam, Phys. Rev. D **84**, 011503 (2011) [arXiv:1104.0163 [nucl-th]].
- [5] L. M. Abreu, D. Cabrera, F. J. Llanes-Estrada and J. M. Torres-Rincon, Ann. Phys. **326**, 2737 (2011) [arXiv:1104.3815 [hep-ph]].
- [6] L. Tolos and J. M. Torres-Rincon, Phys. Rev. D **88**, 074019 (2013) [arXiv:1306.5426 [hep-ph]].
- [7] J. M. Torres-Rincon, L. M. Abreu, D. Cabrera, F. J. Llanes-Estrada and L. Tolos, arXiv:1312.3536 [hep-ph].
- [8] S. K. Das, S. Ghosh, S. Sarkar and J. -eAlam, Phys. Rev. D **85**, 074017 (2012) [arXiv:1109.3359 [hep-ph]].
- [9] L. M. Abreu, D. Cabrera and J. M. Torres-Rincon, Phys. Rev. D **87**, 034019 (2013) [arXiv:1211.1331 [hep-ph]].
- [10] C. Garcia-Recio, J. Nieves, O. Romanets, L. L. Salcedo and L. Tolos, Phys. Rev. D **87**, 034032 (2013) [arXiv:1210.4755 [hep-ph]].
- [11] <http://www.bnl.gov/rhic/>
- [12] <http://home.web.cern.ch/topics/large-hadron-collider>
- [13] <http://www.gsi.de/en/research/fair.htm>
- [14] C. Garcia-Recio, V. K. Magas, T. Mizutani, J. Nieves, A. Ramos, L. L. Salcedo and L. Tolos, Phys. Rev. D **79**, 054004 (2009) [arXiv:0807.2969 [hep-ph]].
- [15] D. Gamermann, C. Garcia-Recio, J. Nieves, L. L. Salcedo and L. Tolos, Phys. Rev. D **81**, 094016 (2010) [arXiv:1002.2763 [hep-ph]].
- [16] O. Romanets, L. Tolos, C. Garcia-Recio, J. Nieves, L. L. Salcedo and R. G. E. Timmermans, Phys. Rev. D **85**, 114032 (2012). [arXiv:1202.2239 [hep-ph]].
- [17] C. Garcia-Recio, J. Nieves, O. Romanets, L. L. Salcedo and L. Tolos, Phys. Rev. D **87**, 074034 (2013) [arXiv:1302.6938 [hep-ph]].
- [18] J. A. Oller and E. Oset, Nucl. Phys. A **620**, 438-456 (1997) [hep-ph/9702314].
- [19] J. A. Oller and U. G. Meissner, Phys. Lett. B **500**, 263 (2001) [hep-ph/0011146].
- [20] M. F. M. Lutz and M. Soyeur, Nucl. Phys. A **813**, 14 (2008) [arXiv:0710.1545 [hep-ph]].
- [21] F. -K. Guo, C. Hanhart, S. Krewald and U. -G. Meissner, Phys. Lett. B **666**, 251 (2008) [arXiv:0806.3374 [hep-ph]].
- [22] F. -K. Guo, C. Hanhart and U. -G. Meissner, Eur. Phys. J. A **40**, 171 (2009) [arXiv:0901.1597 [hep-ph]].
- [23] L. S. Geng, N. Kaiser, J. Martin-Camalich and W. Weise, Phys. Rev. D **82**, 054022 (2010) [arXiv:1008.0383 [hep-ph]].
- [24] J. Beringer *et al.* (Particle Data Group), Phys. Rev. D **86**, 010001 (2012)
- [25] F. -K. Guo, P. -N. Shen, H. -C. Chiang, R. -G. Ping and B. -S. Zou, Phys. Lett. B **641**, 278 (2006) [hep-ph/0603072].
- [26] E. E. Kolomeitsev and M. F. M. Lutz, Phys. Lett. B **582**, 39 (2004) [hep-ph/0307133].
- [27] F. -K. Guo, P. -N. Shen and H. -C. Chiang, Phys. Lett. B **647**, 133 (2007) [hep-ph/0610008].
- [28] R. Aaij *et al.* [LHCb Collaboration], Phys. Rev. Lett. **109**, 172003 (2012) [arXiv:1205.3452 [hep-ex]].
- [29] S. Capstick and N. Isgur, Phys. Rev. D **34**, 2809 (1986)
- [30] H. Garcilazo, J. Vijande and A. Valcarce, J. Phys. G **34**, 961 (2007) [hep-ph/0703257].
- [31] D. Ebert, R. N. Faustov and V. O. Galkin, Phys. Lett. B **659**, 612 (2008) [arXiv:0705.2957 [hep-ph]].
- [32] M. Karliner, B. Keren-Zur, H. J. Lipkin and J. L. Rosner, Annals Phys. **324**, 2 (2009) [arXiv:0804.1575 [hep-ph]].
- [33] W. Roberts and M. Pervin, Int. J. Mod. Phys. A **23**, 2817 (2008) [arXiv:0711.2492 [nucl-th]].
- [34] Y. Yamaguchi, S. Ohkoda, A. Hosaka, T. Hyodo and S. Yasui, arXiv:1402.5222 [hep-ph].
- [35] W. H. Liang, C. W. Xiao and E. Oset, arXiv:1401.1441 [hep-ph].
- [36] L.D. Landau and E.M. Lifshitz and L.P. Pitaevskii, *Course of Theoretical Physics. vol. 10: Physical Kinetics*, (Pergamon Press, 1981)
- [37] <http://nica.jinr.ru/>
- [38] T. Lang, H. van Hees, J. Steinheimer and M. Bleicher, arXiv:1211.6912 [hep-ph].
- [39] T. Lang, H. van Hees, J. Steinheimer and M. Bleicher, arXiv:1305.1797 [hep-ph].
- [40] L. V. Bravina, I. Arsene, M. S. Nilsson, K. Tywoniuk, E. E. Zabrodin, J. Bleibel, A. Faessler and C. Fuchs *et al.*, Phys. Rev. C **78**, 014907 (2008) [arXiv:0804.1484 [hep-ph]].
- [41] S. Ejiri, F. Karsch, E. Laermann and C. Schmidt, Phys. Rev. D **73**, 054506 (2006) [hep-lat/0512040].
- [42] J. Adams *et al.* [STAR Collaboration], Phys. Rev. C **71**, 044906 (2005) [nucl-ex/0411036].
- [43] K. Aamodt *et al.* [ALICE Collaboration], Phys. Lett. B **696**, 328 (2011) [arXiv:1012.4035 [nucl-ex]].